

Emergence of multivariate climate change signals

Article

Published Version

Creative Commons: Attribution 4.0 (CC-BY)

Open Access

King, A. D. ORCID: <https://orcid.org/0000-0001-9006-5745>,
Harrington, L. J. ORCID: <https://orcid.org/0000-0002-1699-6119>,
Hawkins, E. ORCID: <https://orcid.org/0000-0001-9477-3677>,
Paik, S. ORCID: <https://orcid.org/0000-0003-3655-4227>,
Lieber, R., Min, S.-K. ORCID: <https://orcid.org/0000-0002-6749-010X> and Borowiak, A. R. (2024) Emergence of multivariate climate change signals. *Environmental Research Letters*, 19 (9). 094018. ISSN 1748-9326 doi: <https://doi.org/10.1088/1748-9326/ad677f> Available at <https://centaur.reading.ac.uk/117593/>

It is advisable to refer to the publisher's version if you intend to cite from the work. See [Guidance on citing](#).

To link to this article DOI: <http://dx.doi.org/10.1088/1748-9326/ad677f>

Publisher: IOP Science

All outputs in CentAUR are protected by Intellectual Property Rights law, including copyright law. Copyright and IPR is retained by the creators or other copyright holders. Terms and conditions for use of this material are defined in the [End User Agreement](#).

www.reading.ac.uk/centaur

CentAUR

Central Archive at the University of Reading

Reading's research outputs online

LETTER • **OPEN ACCESS**

Emergence of multivariate climate change signals

To cite this article: Andrew D King *et al* 2024 *Environ. Res. Lett.* **19** 094018

View the [article online](#) for updates and enhancements.

You may also like

- [Footprint tools tiptoeing towards nitrogen sustainability](#)
James N Galloway, Rachel E Michaels, Elizabeth A Castner et al.
- [Can the court bridge the gap? Public perception of economic vs. generational inequalities in climate change mitigation policies](#)
Nanna Lauritz Schönhage, Theresa Wieland, Luna Bellani et al.
- [Non-linear media in weakly curved spacetime: optical solitons and probe pulses for gravimetry](#)
Alessio Belenchia, Felix Spengler, Dennis Rätzel et al.

ENVIRONMENTAL RESEARCH
LETTERS

LETTER

Emergence of multivariate climate change signals

OPEN ACCESS

RECEIVED
10 April 2024REVISED
17 July 2024ACCEPTED FOR PUBLICATION
25 July 2024PUBLISHED
12 August 2024

Original content from
this work may be used
under the terms of the
[Creative Commons
Attribution 4.0 licence](#).

Any further distribution
of this work must
maintain attribution to
the author(s) and the title
of the work, journal
citation and DOI.

Andrew D King^{1,2,*} , Luke J Harrington³ , Ed Hawkins⁴ , Seungmok Paik⁵ , Ruby Lieber^{1,6} ,
Seung-Ki Min⁷ and Alexander R Borowiak^{1,6} ¹ School of Geography, Earth and Atmospheric Science, University of Melbourne, Melbourne, Victoria, Australia² ARC Centre of Excellence for 21st Century Weather, Melbourne, Victoria, Australia³ Te Aka Mātuaatua School of Science, University of Waikato, Hillcrest, Hamilton, New Zealand⁴ National Centre for Atmospheric Science, Department of Meteorology, University of Reading, Reading, United Kingdom⁵ Irreversible Climate Change Research Center, Yonsei University, Seoul, Republic of Korea⁶ ARC Centre of Excellence for Climate Extremes, Melbourne, Victoria, Australia⁷ Division of Environmental Science and Engineering, Pohang University of Science and Technology, Pohang, Republic of Korea

* Author to whom any correspondence should be addressed.

E-mail: andrew.king@unimelb.edu.au**Keywords:** climate change emergence, observations, principal component analysis, climate extremesSupplementary material for this article is available [online](#)**Abstract**

The emergence of a climate change signal relative to background variability is a useful metric for understanding local changes and their consequences. Studies have identified emergent signals of climate change, particularly in temperature-based indices with weaker signals found for precipitation metrics. In this study, we adapt climate analogue methods to examine multivariate climate change emergence over the historical period. We use seasonal temperature and precipitation observations and apply a sigma dissimilarity method to demonstrate that large local climate changes may already be identified, particularly in low-latitude regions. The multivariate methodology brings forward the time of emergence by several decades in many areas relative to analysing temperature in isolation. We observed particularly large departures from an early-20th century climate in years when the global warming signal is compounded by an El Niño-influence. The latitudinal dependence in the emergent climate change signal means that lower-income nations have experienced earlier and stronger emergent climate change signals than the wealthiest regions. Analysis based on temperature and precipitation extreme indices finds weaker signals and less evidence of emergence but is hampered by lack of long-running observations in equatorial areas. The framework developed here may be extended to attribution and projections analyses.

1. Introduction

As the planet has warmed, local changes in temperature and precipitation have been observed and, in many regions, attributed to anthropogenic greenhouse gas emissions (IPCC 2021). These changes extend to temperature and precipitation extremes (Easterling *et al* 2016, Paik *et al* 2020) and the observed changes in climate have resulted in many local impacts (Lee *et al* 2023). There are a variety of ways that these changes in climate are estimated statistically, such as trend analyses or shifts in climatological conditions. There have also been attempts to estimate climate change emergence from background

climate variability as an alternative means of measuring local climate changes and their perceptibility (Differbaugh and Scherer 2011, Hawkins and Sutton 2012, Mahlstein *et al* 2012).

Analyses of climate change emergence have been based on various statistical techniques applied to univariate distributions, including:

- Signal-to-noise ratios, often abbreviated to S/N (changes between time periods are computed relative to local climate variability; (Mann and Lees 1996, Hawkins and Sutton 2012, Frame *et al* 2017, Hawkins *et al* 2020)),

- Kolmogorov–Smirnov tests, often abbreviated to K-S tests (comparing distributions of a variable between the past and present, or present and future; (Mahlstein *et al* 2011, 2012, King *et al* 2015)),
- Probability ratios (examining changes in likelihood of extreme events between time periods; (Harrington *et al* 2016, King *et al* 2016)).

Climate change emergence statistics are of relevance to many climate impacts, particularly ecosystems, as an indicator of where impacts may be particularly extreme (Deutsch *et al* 2008, Beaumont *et al* 2011).

Climate change emergence statistics allow for changes to be examined in the context of local climate variability which is strongly spatially heterogeneous and differs between variables. Thus, the patterns of emergence are very different from those of simple long-term trends. For example, trends in seasonal temperatures are strongest over Northern Hemisphere high latitude regions and typically greater over land than ocean (figure S1). However, interannual variability is also generally greater over land and high-latitude regions of the Northern Hemisphere in particular (Hawkins and Sutton 2012, Hawkins *et al* 2020). As a result, the emergence of warming relative to background variability is clearest in low-latitude areas (Mahlstein *et al* 2011, Hawkins *et al* 2020). As mid-to-high latitude regions tend to be wealthier than equatorial areas, there is also a tendency for the poorest areas of the world to be experiencing the clearest and earliest emergence of detectable warming (Harrington *et al* 2016, King and Harrington 2018). For precipitation, trends are more spatially variable (figure S2), and emergence tends to be harder to detect, but there is some evidence of northern high-latitude increases in precipitation already emerging from noise (Hawkins *et al* 2020).

While existing univariate climate change emergence measures are useful for examining climate changes with respect to a relevant variable, it is also of interest to consider changes as a function of more than one variable at a time rather than considering temperature, precipitation or another variable in isolation. Subtle shifts in multiple variables concurrently could result in larger impacts (Zscheischler *et al* 2018) and focussing on univariate emergence risks understating the climate changes experienced in a given location. Indeed, Mahony and Cannon (2018) showed that changes in precipitation coupled with temperature amplify the climate change signal in the warm season. Also, Abatzoglou *et al* (2020) found that considering changes across multiple ecosystem-relevant variables together increased the magnitude of identified changes relative to univariate analysis.

Climate analogues have been used to highlight how a location's climate may change in future and

become more similar to another location's present-day climate (Williams *et al* 2007, Veloz *et al* 2012, Fitzpatrick and Dunn 2019). Climate analogues are typically computed across multiple variables (usually seasonal average temperature and precipitation) to represent more than one aspect of the climate system. Climate analogues are often used as a communication tool and are also applied to impacts studies focussed on ecosystems (Povak and Manley 2023).

In this study we explore the possibility of adapting a climate analogue method to examine emergence of climate changes in a multivariate framework and assess its advantages in identifying climate change signals over the typical univariate analysis. In this instance a baseline climate (temperature and precipitation) is established at each location in the early 20th century and changes from the baseline are tracked at that location. We use observation-based climate datasets as well as information representing aspects of exposure and vulnerability to establish the utility of our proposed framework.

2. Data and methods

2.1. Observational datasets

This study focusses on applying a novel framework for climate change emergence to observational datasets. The majority of the analysis focuses on climate change emergence of seasonal means. We use seasonal-average temperature and precipitation data from the Berkeley Earth Surface Temperature (BEST; Rohde *et al* 2013, Rohde and Hausfather 2020) and the Global Precipitation Climatology Centre (GPCC; Schneider *et al* 2014), respectively. Both BEST and GPCC datasets have been widely used in climate change studies, including for analysis of univariate emergence (Hawkins *et al* 2020). The seasons are defined as March–May (MAM), June–August (JJA), September–November (SON) and December–February (DJF). Analysis was performed over the common 1901–2022/23 period (March 1901 to February 2023). Both datasets were analysed on native regular 1° grids.

Analysis of emergence in climate extreme indices was also conducted by using the highest daily maximum temperature (TXx), lowest daily minimum temperature (TNn) and maximum 1-day precipitation (Rx1day) in each season. These indices were computed from the HadEX3 gridded observational product (Dunn *et al* 2020) which was analysed on its native 1.25° latitude × 1.875° longitude grid.

The BEST and GPCC datasets are near spatially complete over land, but HadEX3 has many gaps in coverage, so the same analysis was performed on temperature and precipitation means and extremes from the ensemble-mean Twentieth Century Reanalysis version 3 (20CR; Compo *et al* 2011, Slivinski *et al* 2019) for comparison. Analysis

with 20CR was conducted for 1901–2015 only as 2015 is when the dataset finishes. The 20CR was constructed by running an atmospheric model constrained by observed sea surface temperatures (SSTs) and surface pressure observations. Even though it is spatially complete it is more accurate where and when observations are assimilated locally. Thus, results derived from 20CR are masked for only locations with an average of at least one observation per month over the 1901–1930 period which is used as a baseline as described in section 2.2. The analysis of 20CR was on its native regular 1° grid.

Effects of climate variability on multivariate climate changes were examined by using the Niño-3.4 index to represent the El Niño-southern oscillation (ENSO). This was calculated from SSTs in the HadISST dataset (Rayner *et al* 2003). Monthly values of Niño-3.4 region-average SSTs were computed and detrended by taking anomalies from a centred moving 15-year window. July–June average values were calculated, to ensure distinct ENSO events were captured, and the standard deviation was used to classify ENSO events. Values above $+0.5\sigma$ were defined as El Niño and values below -0.5σ were defined as La Niña with all other events defined as ENSO-neutral. The method described in section 2.2 provides values representing 12-month periods for studying multivariate emergence, so an ENSO classification based on 12-month windows that does not combine different events is of most use and this is why the July–June average is used.

Analysis of exposure and vulnerability to emergence of multivariate climate change signals was examined using population and gross domestic product (GDP) data. Estimates of these variables for the year 2020 were extracted from the NASA Socioeconomic Data and Applications Centre (CIESIN 2018). These data were aggregated onto a 1° grid to correspond to the grid of the BEST and GPCP datasets. The GDP per capita is simply derived as the GDP divided by the total population in each gridcell. There are many indices that could be used to represent vulnerability, such as Human Development Index (HDI). Both GDP per capita and HDI have been applied in climate change analyses in identifying inequalities of climate change experience or understanding of climate variability (e.g. Lieber *et al* 2022, King *et al* 2023). Locations were assigned by their income decile (figure S3) for the analysis of exposure and vulnerability.

2.2. Method for estimating local multivariate change

As the aim of this analysis was to examine climate change emergence with respect to multiple variables at once, standard methods, such as S/N ratios, were deemed unsuitable. An adaptation to an approach typically used in climate analogue studies was taken instead. Early analogue studies used the Standardised

Euclidean Distance (Williams *et al* 2007, Veloz *et al* 2012), but this places equal weight on all variables and does not account for covariance, so a new more robust method for analogue analysis was proposed by Mahony *et al* (2017). The sigma dissimilarity method implicitly accounts for covariance between variables and has been applied in many climate analogues analyses. The framework used in this analysis is adapted from the method of Mahony *et al* (2017), King (2023) and Paik *et al* (2024) where more detailed descriptions of the sigma dissimilarity calculation may be found. The steps taken are summarised here for the mean variable analysis based on temperature (from BEST) and precipitation (from GPCP) together for a given location. This analysis is thus being performed on an array of eight vectors (MAM, JJA, SON and DJF average temperature and precipitation) each of 122 values (1901–2022/23):

1. Firstly, a cube-root transformation was applied to all precipitation data to decrease skewness in each precipitation timeseries. This transformation has the effect of making the timeseries more gaussian which is useful for subsequent steps.
2. The seasonal-average temperature and cube-root seasonal-average precipitation timeseries for the entire 1901–2022/23 period were standardised using the mean and standard deviation calculated for each season in the baseline 1901–1930 period. For example, the entire MAM temperature timeseries was standardised using the mean and standard deviation of MAM temperatures for 1901–1930. The 1901–1930 period is a pragmatic choice of baseline representing an early-industrial climate state for which adequate observational data exist.
3. Principal component analysis was performed on the sub-array of standardised seasonal temperature and precipitation timeseries for the 1901–1930 baseline period (i.e. an array of 8 vectors of 30 values each).
4. Arrays for the entire standardised seasonal temperature and precipitation timeseries from 1901–2022/23 were projected on to the extracted principal components (PCs).
5. The Mahalanobis distance (Mahalanobis 2018) was computed for each year (March–February to match definition of seasons) in the transformed timeseries compiled in step 4. The Mahalanobis distance is computed as:

$$D_j = \sqrt{\sum_{n=1}^N \frac{(\bar{z}_n - y_{jn})^2}{s_n^2}},$$

where N is the number of PCs, \bar{z}_n is the mean of each PC projected on to the standardised variables for 1901–1930, y_{jn} is each PC projected on to the standardised variables for each year over 1901–2022/23, and s_n is the standard deviation of each

PC projected on to the standardised variables for 1901–1930. For the example of seasonal-average temperature and precipitation, $N = 8$.

6. The Mahalanobis Distance was converted to a sigma dissimilarity metric using the Chi-distribution where the mean, μ , is:

$$\mu = \frac{\sqrt{2}\Gamma\left(\frac{N+1}{2}\right)}{\Gamma\left(\frac{N}{2}\right)}$$

and the standard deviation, σ , is

$$\sigma = \sqrt{N - \mu^2},$$

where N is the number of PCs. By converting Mahalanobis distance to sigma dissimilarity, results may be compared between analyses where N is different.

These steps were repeated for each gridcell with available observational data. The framework was also applied to different sets of variables and other datasets to aid in interpretation and to establish the robustness of the results:

- seasonal temperatures only (BEST),
- seasonal precipitation only (GPCC),
- seasonal temperature and precipitation (20CR),
- seasonal temperatures only (20CR),
- seasonal precipitation only (20CR),
- seasonal TXx, TNn and Rx1day (HadEX3),
- seasonal TXx, TNn and Rx1day (20CR).

While the method here largely follows from previous work there are some differences that should be noted. Here, the climate at each location is being compared with its own baseline rather than the comparison being made between locations. Also, Mahony *et al* (2017) suggest use of separate seasonal-average maximum and minimum temperatures may be more suitable for characterising a baseline climate state and identifying changes compared with using only seasonal-mean temperatures. There are BEST maximum and minimum temperature data products over land only. The decision to include ocean areas for the temperature-only analysis meant we chose to use seasonal-mean temperatures for this analysis. Example timeseries of seasonal temperature and precipitation and associated sigma dissimilarity values are shown in figure S4 for the gridcell over Melbourne, Australia.

2.3. Identifying multivariate climate changes

The sigma dissimilarity metric may be used to identify timings and locations where significant changes from the 1901–1930 baseline climate have occurred. At every location with observational data there is an

annual timeseries of the sigma dissimilarity metric (with each value representing the 12-month period from March of one year to February of the next). The average sigma dissimilarity over 30-year periods was computed for 1961–1990 and 1991–2020. The time of emergence was computed as the central year when the 11-year running average of the sigma dissimilarity exceeds a threshold and remains above that threshold for all subsequent values of the 11-year running average. A 2σ threshold was used for most of the time of emergence analysis, but thresholds of 3σ and 4σ were also examined. Dissimilarity of 2σ corresponds to the 95th percentile of the baseline period and may be used to approximate moderately novel climates (Mahony *et al* 2017). Dissimilarity values exceeding 2σ can be thought of as representing climates which are significantly different ($p < 0.05$) from the baseline period and, statistically, very likely to be drawn from different populations. Times of emergence identified after 2010 may well not be permanent as they are near the end of the timeseries (Hawkins *et al* 2014), so these were not plotted. Ideally, a longer period before the end of the observations would be excluded as emergence could be temporary, but any emergence identified by 2010 is at least maintained to the end of the timeseries including 11-year periods with less than 50% overlap. Use of different lengths of running averages have little effect on the results.

As the sigma dissimilarity metric has annual values, individual years or frequencies of departures from the baseline may also be assessed. The frequency of years greater than 2σ , 3σ and 4σ from the 1901–1930 baseline were computed for 1961–1990 and 1991–2020.

Aggregate timeseries were computed to examine global trends, ENSO relationships and population exposure to multivariate climate changes. Global area exceeding 2σ , 3σ and 4σ dissimilarity from location-specific baseline climate was computed for each year, discounting for locations with missing data. The global population exposed to local climate changes greater than 2σ , 3σ and 4σ dissimilarity in each year up to 2023 was also estimated by simply summing the population in the locations exceeding these thresholds. Composites of mean frequency of exceeding 2σ thresholds by ENSO state were plotted for years from 1990 onwards.

In addition to population exposure, vulnerability was also considered. Box-and-whisker plots were compiled for each income decile to examine relationships with various measures of multivariate climate changes (average sigma dissimilarity in 1991–2020, number of years exceeding 2σ difference in 1991–2020, and time of emergence). The purpose of this analysis was to identify whether the inequality

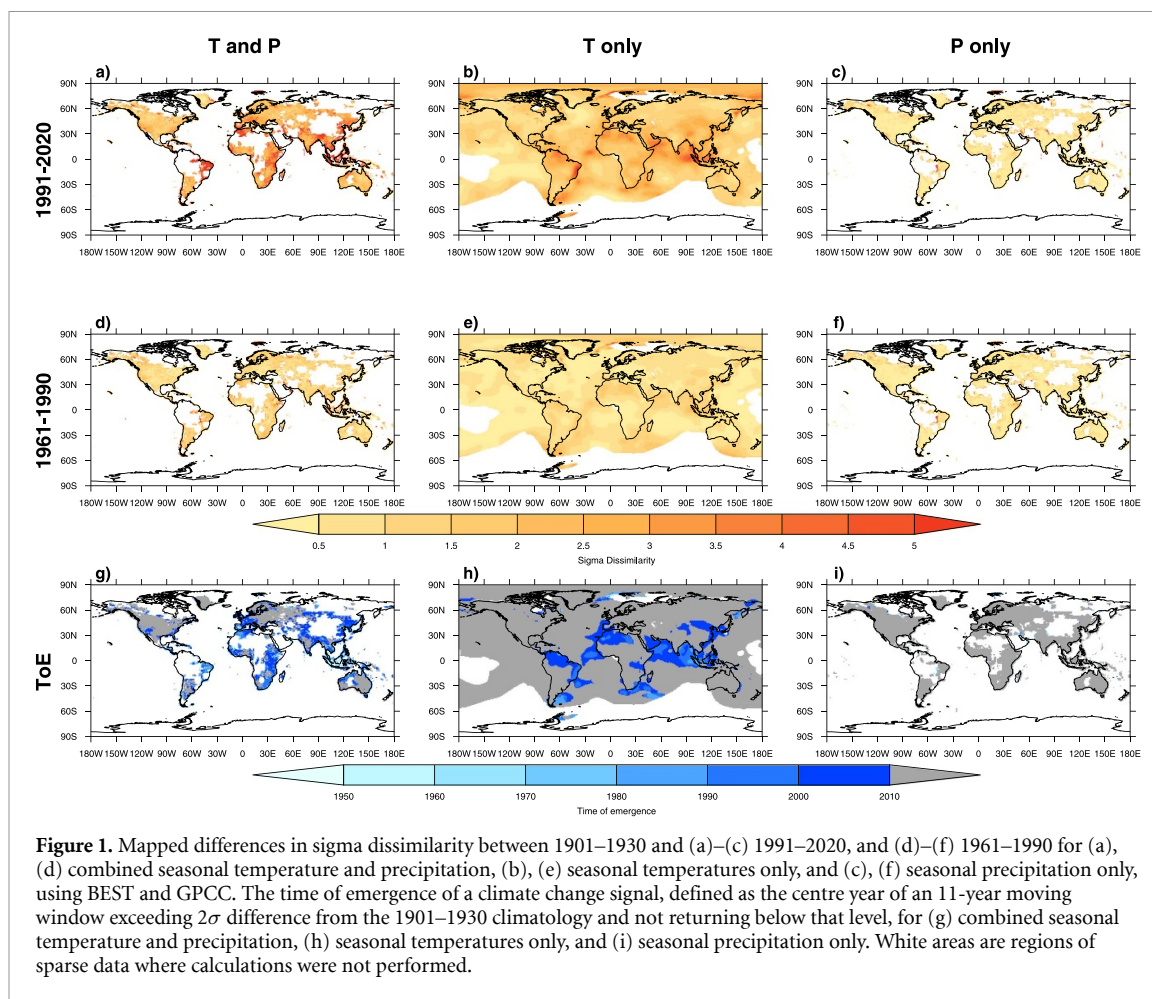


Figure 1. Mapped differences in sigma dissimilarity between 1901–1930 and (a)–(c) 1991–2020, and (d)–(f) 1961–1990 for (a), (d) combined seasonal temperature and precipitation, (b), (e) seasonal temperatures only, and (c), (f) seasonal precipitation only, using BEST and GPCC. The time of emergence of a climate change signal, defined as the centre year of an 11-year moving window exceeding 2σ difference from the 1901–1930 climatology and not returning below that level, for (g) combined seasonal temperature and precipitation, (h) seasonal temperatures only, and (i) seasonal precipitation only. White areas are regions of sparse data where calculations were not performed.

identified previously in univariate climate emergence studies (Mahlstein *et al* 2011, Harrington *et al* 2016, King and Harrington 2018) extends to multivariate climate change patterns.

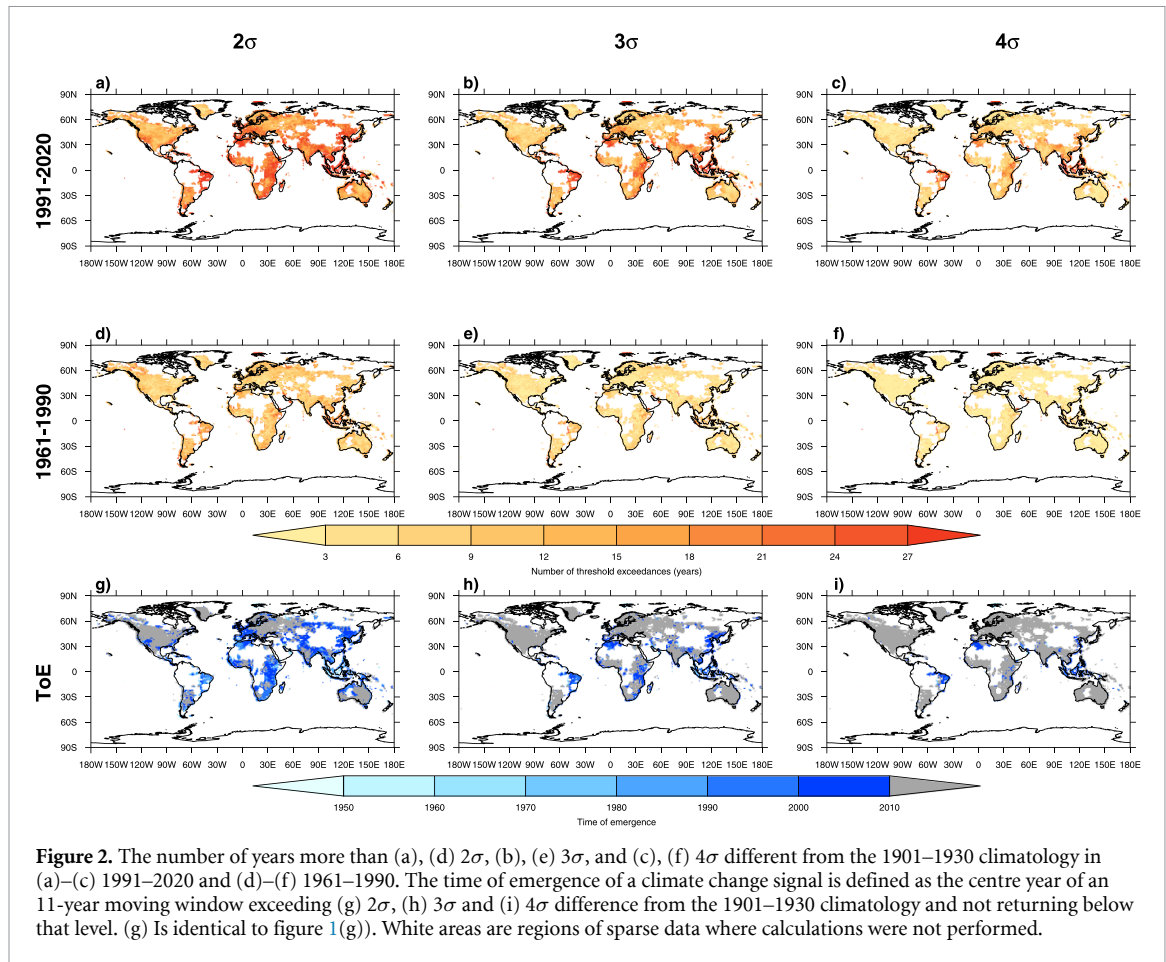
An extremes analysis was performed using HadEX3 and 20CR and the average sigma dissimilarity was computed for 1961–1990 and 1991–2015 relative to the 1901–1930 baseline. The time of emergence was defined in the same way as in the means analysis using the 2σ threshold.

3. Results

The metric of multivariate climate change used here, the sigma dissimilarity, exhibits increasing values over time as temperatures increase and precipitation changes (figures 1(a) and (d)). The average sigma dissimilarity is greater for the 1991–2020 period than 1961–1990 with stronger dissimilarity identified in equatorial regions compared with mid-to-high latitudes. There are observational gaps, but there is still evidence of a strong latitudinal relationship with sigma dissimilarity due to high values in eastern South America, parts of Africa, and the Maritime Continent. When sigma dissimilarity statistics are

computed and analysed for temperature and precipitation separately we see that temperature is dominating the changes in the multivariate sigma dissimilarity values (figures 1(b), (c), (e) and (f)). In both the multivariate and the temperature-only patterns, low-latitude areas have experienced greater climate changes compared with mid-to-high latitudes, in line with previous findings (Mahlstein *et al* 2011, Hawkins and Sutton 2012, Harrington *et al* 2016).

The time of emergence maps reflect the spatial patterns seen in sigma dissimilarity. Earlier emergence is found in low-latitude areas than elsewhere with a lack of emergence in many mid-to-high latitude regions (figure 1(g)). Emergence of temperature changes alone is evident in many low-latitude areas (figure 1(h)), including some ocean locations which are masked in the multivariate analysis due to lack of precipitation data. There is little evidence of precipitation emergence, although some northern high latitude areas are masked for lack of data where there has been some evidence of precipitation emergence in previous work (King *et al* 2015, Hawkins *et al* 2020). Despite the lack of emergence of a precipitation signal, the inclusion of precipitation in the multivariate analysis brings forward the time of emergence



relative to analysis of temperature alone by two to three decades in some areas (figure S5). This is expected as even small changes in one variable will act to increase the overall shift from the baseline climate as represented by the sigma dissimilarity. The physical reasons for this will differ between locations and could include not only increases or decreases in precipitation, but also changes in seasonal cycles.

The frequency of individual years exceeding sigma dissimilarity thresholds increases over time and follows a similar pattern to average sigma dissimilarity with more exceedances in equatorial areas (figure 2). In the 1991–2020 period, most years exhibit departures above 3σ from the reference period in sampled low-latitude areas, particularly eastern South America, Sub-Saharan Africa, and the Maritime Continent. There is a hint of a similar spatial pattern in the 1961–1990 results (figures 2(d)–(f)), but the lack of a signal until the more recent period makes this less clear. Time of emergence analysis based on different sigma dissimilarity thresholds shows the same broad pattern (figures 2(g)–(i)). There are equatorial locations where emergence has occurred using a strict 4σ threshold while large swaths of the mid-to-high latitudes have not yet experienced local climate change emergence even using a less strict threshold of 2σ .

Area and population exposure to multivariate climate changes were examined utilising the annual calculation of the sigma dissimilarity metric. The accelerated trend in area experiencing markedly different climate states from their 1901–1930 baselines is clear with large increases in this area from the 1970s onwards (figures 3(a)–(c)). Between adjacent years there are increases in area experiencing high sigma dissimilarity in El Niño years and small decreases in La Niña years. For the calculation of population exposure, overall 6.7 billion people are estimated to live in areas where the analysis could be conducted due to adequate observational coverage (figures 3(d)–(f)). There is an ENSO relationship with population exposed to high sigma dissimilarity events albeit less clear than in the area average. There has been a marked increase in the proportion of global population living in areas where large local climate changes have occurred relative to their 1901–1930 baseline state. The proportion of the world population exposed to local climate changes exceeding 2, 3 and 4σ from the baseline climates is higher in all years from 2015 onwards than all years prior to 2015.

While ENSO effects are identifiable in global aggregate statistics of departures from baseline climate states, the ENSO relationship with local sigma

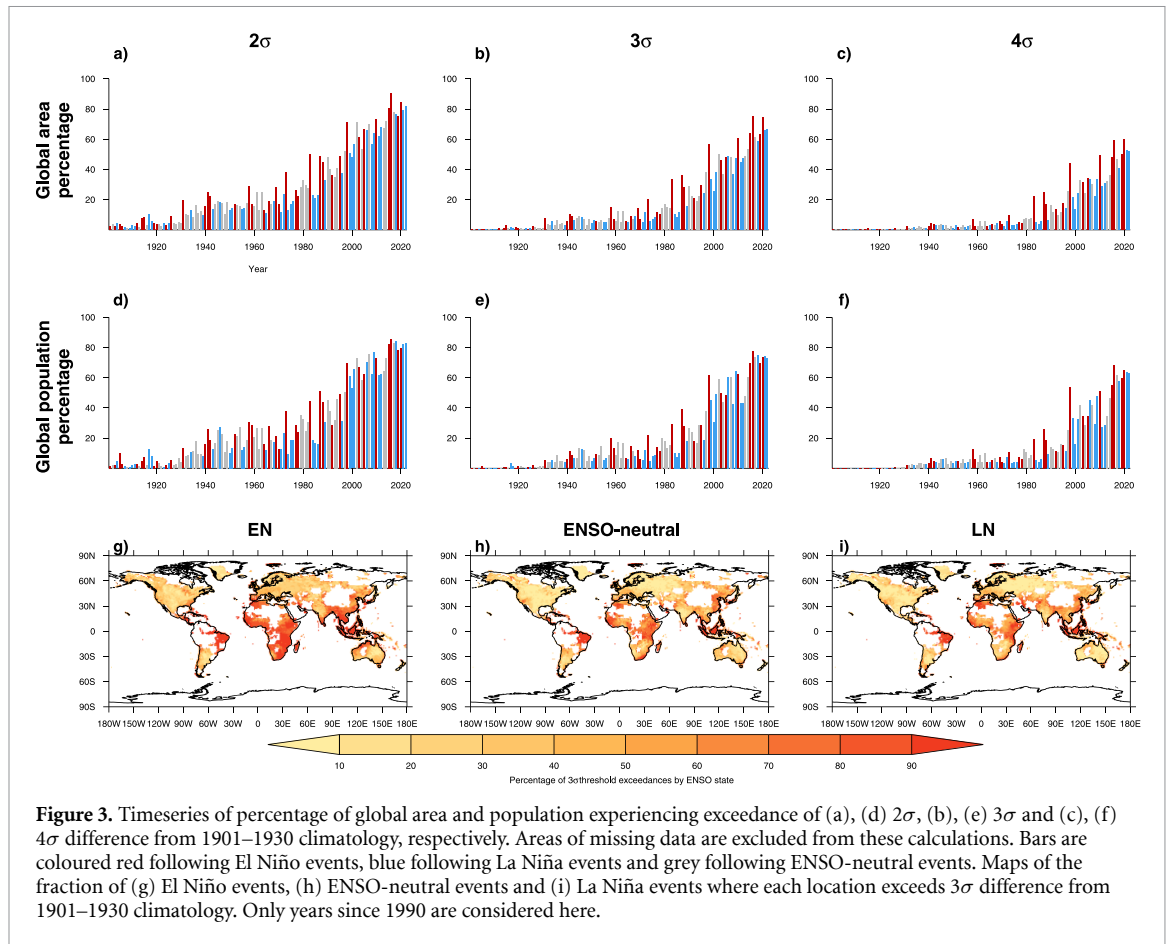


Figure 3. Timeseries of percentage of global area and population experiencing exceedance of (a), (d) 2σ , (b), (e) 3σ and (c), (f) 4σ difference from 1901–1930 climatology, respectively. Areas of missing data are excluded from these calculations. Bars are coloured red following El Niño events, blue following La Niña events and grey following ENSO-neutral events. Maps of the fraction of (g) El Niño events, (h) ENSO-neutral events and (i) La Niña events where each location exceeds 3σ difference from 1901–1930 climatology. Only years since 1990 are considered here.

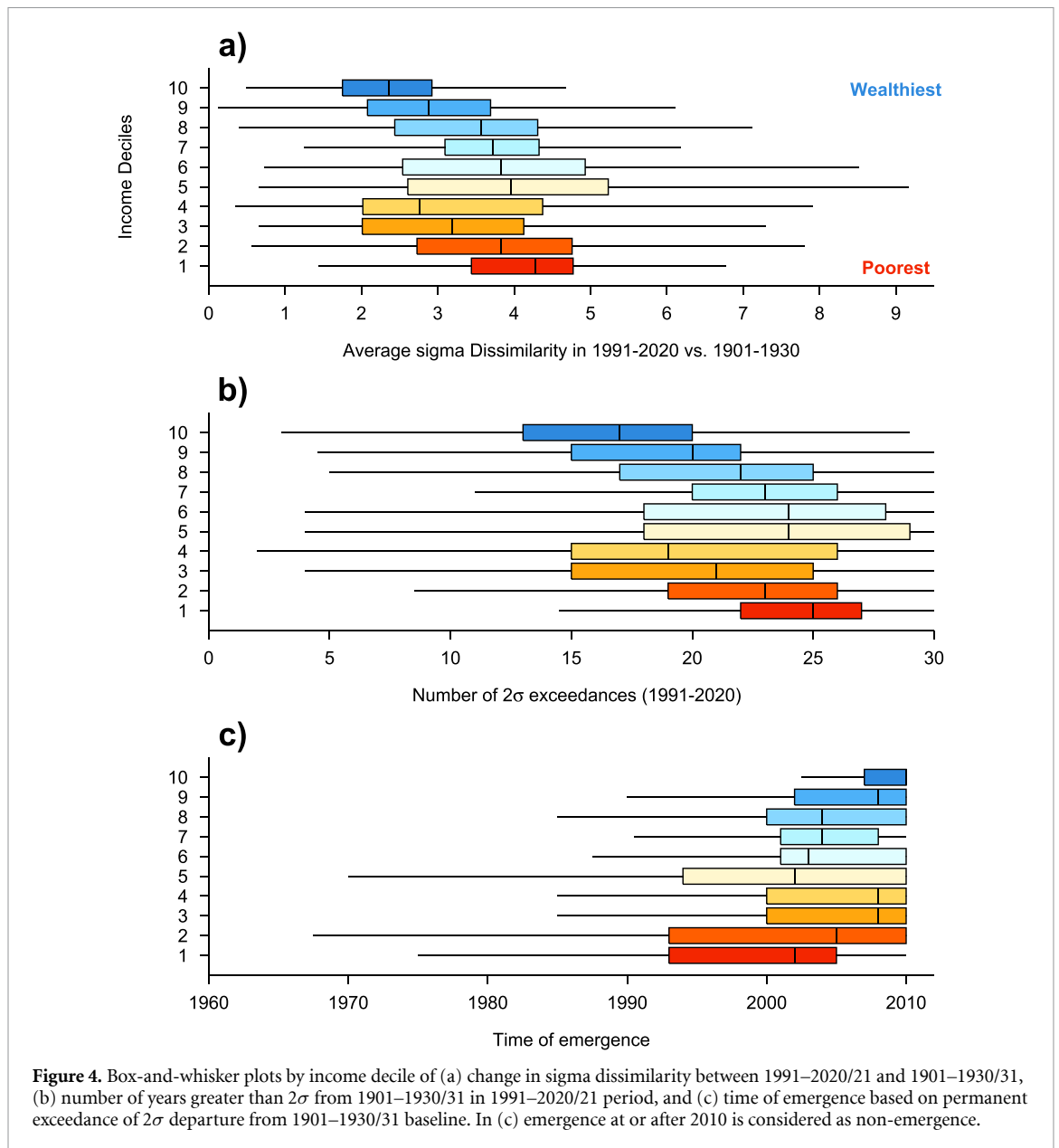
dissimilarity is spatially variable (figures 3(g)–(i) and S6). In southern Africa, southeast Asia and parts of Australia, the occurrence of large climate departures from the reference climate is higher in El Niño years. In parts of central Asia, North and South America and southern Europe, the chance of high sigma dissimilarity years is greater in La Niña. Individual years show large local differences in sigma dissimilarity, but the larger sigma dissimilarity in the tropics remains clear (figure S7).

Given the latitudinal relationship with sigma dissimilarity and the inequalities identified in univariate climate change emergence studies, an analysis of relationships between metrics based on local sigma dissimilarity and local GDP per capita was conducted (figure 4). There is some tendency for lower income regions of the world to have experienced greater change in mean sigma dissimilarity (figure 4(a)), greater frequency of high sigma dissimilarity years (figure 4(b)), and earlier emergence of multivariate climate changes (figure 4(c)). In fact, between the locations of the richest and poorest people by decile, we see substantially different experiences of climate change with non-overlapping interquartile ranges in all three charts. Comparable scatter plots (figure S8) illustrate the same relationships with significant correlations, although this is in part due to the large number of points.

Finally, we examined for changes in extremes by computing sigma dissimilarity statistics based on seasonal values of TXx , TNn and $Rx1day$ (figure 5). Results based on HadEX3 show little evidence of substantial changes in local climate based on these extreme indices. This is in part due to the lack of spatial coverage extending back to the early 20th century. Analysis was repeated for 20CR which shows similar mean climate results as the analysis based on BEST and GPCC (figure S9). The 20CR results are based on greater spatial coverage and suggest some significant changes, particularly in equatorial areas. There is evidence of emergence in tropical areas, but these are generally poorly observed areas of the world, particularly for historical instrumental climate data that acts to constrain 20CR.

4. Discussion and conclusions

In this study we have adapted a framework used to identify climate analogues and applied this to examine for multivariate climate change and emergence. By applying this technique to observational data, we find larger local climate changes and earlier emergence of a climate change signal in tropical regions than at higher latitudes. This is in line with previous climate change emergence analyses (Mahlstein *et al*

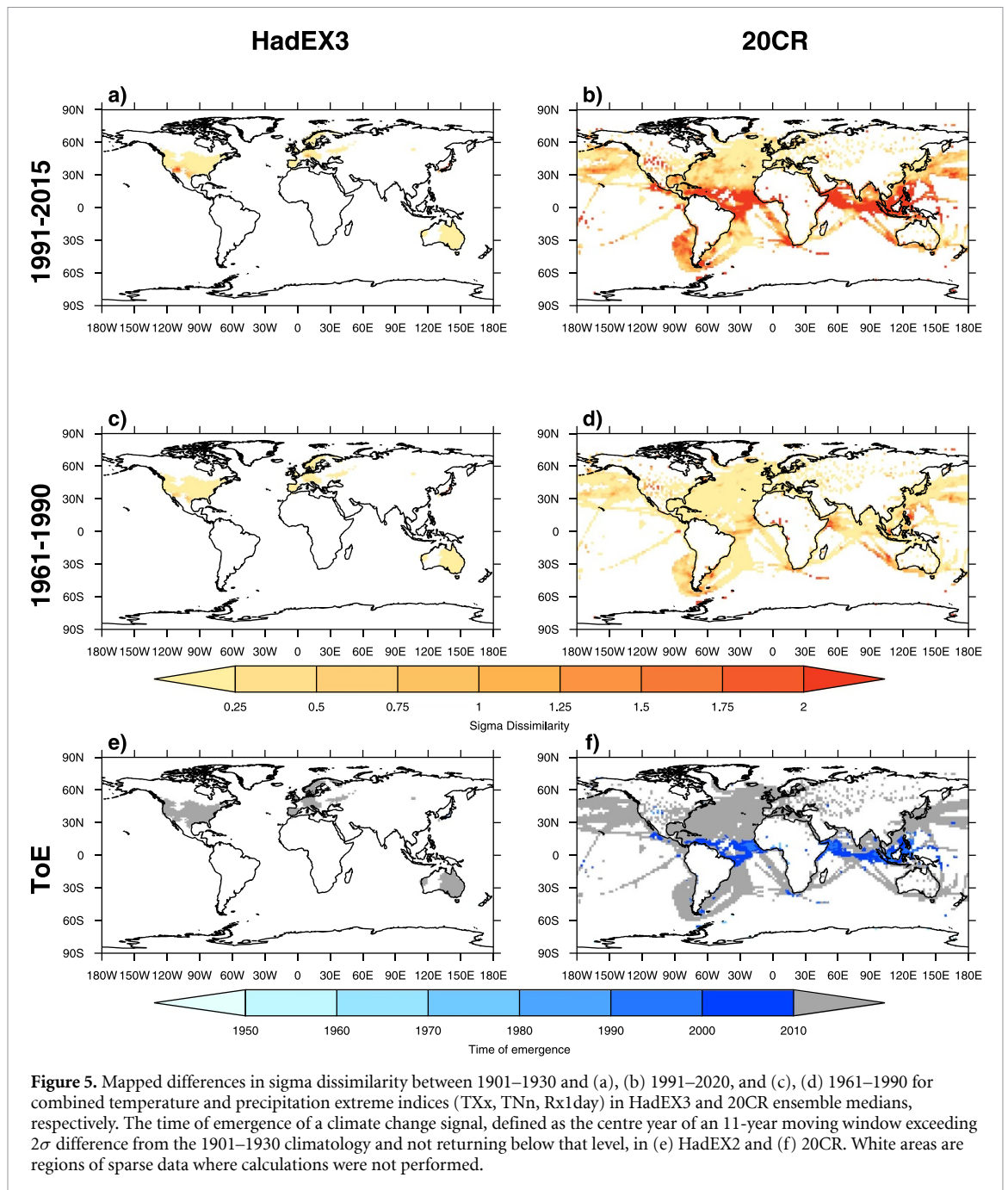


2011, Hawkins and Sutton 2012), although the inclusion of precipitation in the method increases the magnitude of identified changes. Local departures from an early 20th century baseline climate are clearer in some years than others, but on average, across the locations where this analysis was performed, these departures are larger in El Niño years than La Niña years. The dominant pattern of larger local climate changes in the tropics than mid-to-high latitudes gives rise to inequality whereby poorer areas experience earlier emergence of climate change. Analysis of changes in extremes is hampered by lack of long-term observations, but there is some evidence of earlier emergence in tropical areas also.

This study builds on previous climate change emergence work by moving from univariate to multivariate analysis. This allows for a more holistic approach to identification of climate change, but results should be interpreted in the context of known

changes in component variables. The sigma dissimilarity method used here is robust, does not require choices to be made about weighting, and implicitly incorporates covariance information. This method also allows for analysis of individual years and their departures from a baseline climate which is not typically possible using S/N ratios or K–S test-based approaches.

This work also extends the framework proposed for robust detection of climate analogues (Mahony *et al* 2017), which was subsequently applied to identification of observed multivariate climate changes relevant to ecosystems (Abatzoglou *et al* 2020), a step further into analysis of climate emergence. Given the growing focus on multi-hazard or compound events and their changes (Zscheischler *et al* 2018), we hope that our framework for identifying multivariate climate change emergence is useful to the community.



There are caveats to note as well as possible extensions to this work. This study is reliant on the underlying observational data. Masking was performed to restrict analysis to locations with complete data throughout the timeseries, but inhomogeneities have the potential to influence results. There is greater confidence in results in well-observed areas of the world, such as parts of western Europe, North America and southeast Australia, compared with other areas where large changes are identified, such as the Maritime Continent and Sub-Saharan Africa. King (2023) used a recent baseline period to identify historical changes when examining Australian climate analogues, as the sigma dissimilarity calculations are based on a better constrained observational period. While this was not

done here, so that a time of emergence may be estimated, a sensitivity test using a 1991–2020 baseline and examining differences from that period gives a similar pattern of sigma dissimilarity change (figure S10) and this provides some confidence in the overall conclusions of the analysis.

The analysis shown here uses a 1901–1930 baseline and examines for changes since that time. Analysis with different baselines will lead to local differences, but the general geographical patterns appear to be robust. For example, we repeated the analysis on a 1911–1940 baseline, which includes several warm years for the globe in the 1930s and the Dust Bowl period in the central United States (e.g. Donat *et al* 2016, Cowan *et al* 2020). In general, use

of a 1911–1940 baseline makes little difference and the latitudinal variability in sigma dissimilarity and emergence remains (figures S11 and S12).

Use of a 1901–1930 baseline means that our analysis is over a period of significant climate change with the majority of warming due to human influences. As the analysis is only on the observational record, there is no distinction made between changes due to internal climate variability and anthropogenic influence, although given the long period of analysis it is likely to be dominated by human-caused climate change (Haustein *et al* 2019). A model-based analysis could be used to extend this work and estimate anthropogenic and natural changes as well as a time of anthropogenic emergence (King *et al* 2016). Furthermore, the framework used here could be extended to future changes under different greenhouse gas emissions scenarios for the 21st century.

Overall, we believe that the framework outlined here is useful and in applying it to observational data we have identified and quantified multivariate climate change signals that have occurred. Further analyses using this framework may be of use in identifying climate change hotspots and informing associated impacts under continued global warming.

Data availability statement

All datasets used in this study are publicly available: BEST data from <https://berkeleearth.org/data/>, GPCC data from www.dwd.de/EN/ourservices/gpcc/gpcc.html, 20CR data from www.psl.noaa.gov/data/gridded/data.20thC_ReanV3.html, and GDP and population data from <https://sedac.ciesin.columbia.edu/data/set/gpw-v4-population-count-rev11>.

Acknowledgments

A D K received funding from the ARC Centre of Excellence for 21st Century Weather (CE230100012) and the Australian Government through the National Environmental Science Program. L J H acknowledges funding from the New Zealand Ministry for Business, Innovation & Employment's Endeavour Fund Whakahura programme (Grant ID: RTVU1906). S P and S K M receive funding from the National Research Foundation of Korea (NRF) Grant funded by the Korean government (MSIT) (NRF-2018R1A5A1024958, NRF-2021R1C1C2094185).

Conflict of interest

The authors declare no competing interests.

ORCID iDs

Andrew D King  <https://orcid.org/0000-0001-9006-5745>


Luke J Harrington  <https://orcid.org/0000-0002-1699-6119>

Ed Hawkins  <https://orcid.org/0000-0001-9477-3677>

Seungmok Paik  <https://orcid.org/0000-0003-3655-4227>

Ruby Lieber  <https://orcid.org/0000-0003-3196-3080>

Seung-Ki Min  <https://orcid.org/0000-0002-6749-010X>

Alexander R Borowiak  <https://orcid.org/0000-0002-0499-7800>

References

- Abatzoglou J T, Dobrowski S Z and Parks S A 2020 Multivariate climate departures have outpaced univariate changes across global lands *Sci. Rep.* **10** 1–9
- Beaumont L J, Pitman A, Perkins S, Zimmermann N E, Yoccoz N G and Thuiller W 2011 Impacts of climate change on the world's most exceptional ecoregions *Proc. Natl Acad. Sci. USA* **108** 2306–11
- Center for International Earth Science Information Network—CIESIN—Columbia University 2018 Gridded population of the world (GPW), v4: basic demographic characteristics, v4.11 (NASA Socioeconomic Data and Applications Center (SEDAC)) (available at: <https://sedac.ciesin.columbia.edu/data/set/gpw-v4-basic-demographic-characteristics-rev11>)
- Compo G P *et al* 2011 The Twentieth Century Reanalysis Project *Q. J. R. Meteorol. Soc.* **137** 1–28
- Cowan T, Hegerl G C, Schurer A, Tett S F B, Vautard R, Yiou P, Jézéquel A, Otto F E L, Harrington L J and Ng B 2020 Ocean and land forcing of the record-breaking Dust Bowl heatwaves across central United States *Nat. Commun.* **11** 1–9
- Deutsch C A, Tewksbury J J, Huey R B, Sheldon K S, Ghalambor C K, Haak D C and Martin P R 2008 Impacts of climate warming on terrestrial ectotherms across latitude *Proc. Natl Acad. Sci. USA* **105** 6668–72
- Diffenbaugh N S and Scherer M 2011 Observational and model evidence of global emergence of permanent, unprecedented heat in the 20th and 21st centuries *Clim. Change* **107** 615–24
- Donat M G, King A D, Overpeck J T, Alexander L V, Durre I and Karoly D J 2016 Extraordinary heat during the 1930s US Dust Bowl and associated large-scale conditions *Clim. Dyn.* **46** 413–26
- Dunn R J H *et al* 2020 Development of an updated global land in situ-based data set of temperature and precipitation extremes: hadEX3 *J. Geophys. Res. Atmos.* **125** e2019JD032263
- Easterling D R, Kunkel K E, Wehner M F and Sun L 2016 Detection and attribution of climate extremes in the observed record *Weather Clim. Extremes* **11** 17–27
- Fitzpatrick M C and Dunn R R 2019 Contemporary climatic analogs for 540 North American urban areas in the late 21st century *Nat. Commun.* **10** 1–7
- Frame D J, Joshi M M, Hawkins E, Harrington L J and de Roiste M 2017 Population-based emergence of unfamiliar climates *Nat. Clim. Change* **7** 407–11
- Harrington L J, Frame D J, Fischer E M, Hawkins E, Joshi M M and Jones C D 2016 Poorest countries experience earlier anthropogenic emergence of daily temperature extremes *Environ. Res. Lett.* **11** 055007
- Haustein K, Otto F E L, Venema V, Jacobs P, Cowtan K, Hausfather Z, Way R G, White B, Subramanian A and Schurer A P 2019 A limited role for unforced internal

- variability in twentieth-century warming *J. Clim.* **32** 4893–917
- Hawkins E et al 2014 Uncertainties in the timing of unprecedented climates *Nature* **511** E3–E5
- Hawkins E, Frame D J, Harrington L, Joshi M M, King A D, Rojas M and Sutton R 2020 Observed Emergence of the Climate Change Signal: From the Familiar to the Unknown *Geophys. Res. Lett.* **47** e2019GL086259
- Hawkins E and Sutton R 2012 Time of emergence of climate signals *Geophys. Res. Lett.* **39** L01702
- IPCC 2021 Summary for policymakers *Climate Change 2021: The Physical Science Basis. Contribution of Working Group I to the Sixth Assessment Report of the Intergovernmental Panel on Climate Change* ed V Masson-Delmotte, et al (Cambridge University Press) pp 3–32
- King A D 2023 Identifying historical climate changes in Australia through spatial analogs *Environ. Res. Lett.* **18** 044018
- King A D, Black M T, Min S-K, Fischer E M, Mitchell D M, Harrington L J and Perkins-Kirkpatrick S E 2016 Emergence of heat extremes attributable to anthropogenic influences *Geophys. Res. Lett.* **43** 3438–43
- King A D, Donat M G, Fischer E M, Hawkins E, Alexander L V, Karoly D J, Dittus A J, Lewis S C and Perkins S E 2015 The timing of anthropogenic emergence in simulated climate extremes *Environ. Res. Lett.* **10** 094015
- King A D, Douglas H, Harrington L J, Hawkins E and Borowiak A R 2023 Climate change emergence over people's lifetimes *Environ. Res.: Clim.* **2** 041002
- King A D and Harrington L J 2018 The inequality of climate change from 1.5 to 2 °C of Global Warming *Geophys. Res. Lett.* **45** 5030–3
- Lee H et al 2023 Synthesis report of the IPCC sixth assessment report (AR6) *Intergovernmental Panel on Climate Change* (Cambridge University Press)
- Lieber R, King A D, Brown J, Ashcroft L, Freund M and McMichael C 2022 ENSO Teleconnections More Uncertain in Regions of Lower Socioeconomic Development *Geophys. Res. Lett.* **49** e2022GL100553
- Mahlstein I, Hegerl G and Solomon S 2012 Emerging local warming signals in observational data *Geophys. Res. Lett.* **39** L21711
- Mahlstein I, Knutti R, Solomon S and Portmann R W 2011 Early onset of significant local warming in low latitude countries *Environ. Res. Lett.* **6** 034009
- Mahony C R and Cannon A J 2018 Wetter summers can intensify departures from natural variability in a warming climate *Nat. Commun.* **9** 1–9
- Mahony C R, Cannon A J, Wang T and Aitken S N 2017 A closer look at novel climates: new methods and insights at continental to landscape scales *Glob. Change Biol.* **23** 3934–55
- Mann M E and Lees J M 1996 Robust estimation of background noise and signal detection in climatic time series *Clim. Change* **33** 409–45
- Paik S, An S-I, King A D, Kim S-K and Min S-K 2024 Understanding climate changes in East Asia and Europe based on spatial climate analogs *Environ. Res. Lett.* **19** 044036
- Paik S, Min S K, Zhang X, Donat M G, King A D and Sun Q 2020 Determining the Anthropogenic Greenhouse Gas Contribution To The Observed Intensification Of Extreme Precipitation *Geophys. Res. Lett.* **47** e2019GL086875
- Povak N A and Manley P N 2023 Evaluating climate change impacts on ecosystem resources through the lens of climate analogs *Front. For. Glob. Change* **6** 1286980
- Rayner N A, Parker D E, Horton E B, Folland C K, Alexander L V, Rowell D P, Kent E C and Kaplan A 2003 Global analyses of sea surface temperature, sea ice, and night marine air temperature since the late nineteenth century *J. Geophys. Res.* **108** 4407
- Reprint of 1936: Mahalanobis P C 2018 On the generalized distance in statistics *Sankhya A* **80** 1–7
- Rohde R A and Hausfather Z 2020 The Berkeley Earth land/ocean temperature record *Earth Syst. Sci. Data* **12** 3469–79
- Rohde R A, Muller R, Jacobsen R, Perlmutter S and Mosher S 2013 Berkeley earth temperature averaging process *Geoinf. Geostat.* **1** 20–100
- Schneider U, Becker A, Finger P, Meyer-Christoffer A, Ziese M and Rudolf B 2014 GPCC's new land surface precipitation climatology based on quality-controlled in situ data and its role in quantifying the global water cycle *Theor. Appl. Climatol.* **115** 15–40
- Slivinski L C et al 2019 Towards a more reliable historical reanalysis: improvements for version 3 of the Twentieth Century Reanalysis system *Q. J. R. Meteorol. Soc.* **145** 2876–908
- Veloz S, Williams J W, Lorenz D, Notaro M, Vavrus S and Vimont D J 2012 Identifying climatic analogs for Wisconsin under 21st-century climate-change scenarios *Clim. Change* **112** 1037–58
- Williams J W, Jackson S T and Kutzbach J E 2007 Projected distributions of novel and disappearing climates by 2100 AD *Proc. Natl Acad. Sci. USA* **104** 5738–42
- Zscheischler J et al 2018 Future climate risk from compound events *Nat. Clim. Change* **8** 469–77